Journal of Materials Chemistry B

Accepted Manuscript

ROYAL SOCIETY OF CHEMISTRY

www.rsc.org/materialsB

Journal Name

RSCPublishing

ARTICLE

Triethylphosphite as a network forming agent enhances *in-vitro* biocompatibility and corrosion protection of hybrid organic-inorganic sol-gel coatings for Ti6Al4V alloys

Cite this: DOI: 10.1039/x0xx00000x

Received 00th January 2012,
Accepted 00th January 2012

DOI: 10.1039/x0xx00000x

www.rsc.org/

A. A. El hadad[a], V. Barranco[b], A. Jiménez-Morales[c], G. J. Hickman[d], J. C. Galván[a] and C. C. Perry*[d]

The biocompatibility and life of metallic implants can be enhanced through improving the biocompatibility and corrosion protection characteristics of the coatings used with these materials. In this study, triethylphosphite (TEP) was used to introduce phosphorus into organic-inorganic hybrid silica based sol-gel coatings prepared using γ-methacryloxypropyltrimethoxysilane and tetramethylorthosilicate. Addition of TEP dramatically increased the rate of intermolecular condensation and resulted in materials showing greater cross-linking. Protein (fibrinogen) uptake, osteoblast *in vitro* biocompatibility and corrosion resistance was enhanced in coatings containing TEP. Although higher concentrations of phosphorus supported the greatest improvement in biocompatibility, a compromise in the phosphorus concentration used would be required if corrosion resistance was most desirable parameter for optimisation. Films prepared by dip coating on Ti6Al4V alloys from these sols offer a promising alternative to wholly metallic prostheses

Introduction

Titanium and its alloys such as Ti6Al4V are commonly used materials for *in vivo* applications due in part to their corrosion resistance and the inert character of the naturally forming oxide layer.[1] However, this passive layer may be disrupted at very low shear stresses, including rubbing of materials against soft tissues.[2] As a consequence, titanium and other alloying metal ions such as aluminium and vanadium are released from the implant and accumulate in nearby tissues from the aggressive action of biological fluids.[2] Ions associated with corrosion of the Ti6Al4V surface inhibit osteoblast proliferation and growth *in vitro*, suggesting that ions released from implants *in vivo* may be implicated in implant failure.[3]

Coating the alloy with a bioactive material provides a physical barrier between the metal surface and the aggressive species present in biological fluids and at the same time may provide a mechanically strong bond with living bone.[4] Several coating techniques have been adopted to improve the corrosion resistance of metal alloys by deposition of thin films on the metallic surface. These include plasma spray,[5] chemical conversion[6] and the sol–gel method,[7] etc. Among the above, the sol-gel technique has attracted considerable interest as a non-toxic substitute for chromium (VI) treatment. This method offers many advantages (high purity and homogeneity, low processing temperatures, reduced thickness, simple and cheap preparation) for the production of coatings on materials including Ti6Al4V implants.[8, 9]

Organic–inorganic hybrids based on siloxane bonded units prepared by a sol-gel route have unique properties that arise from the synergism between the properties of both components.[10] We have previously reported on the use of hydroxyapatite in organic–inorganic hybrids to improve biocompatibility and corrosion resistance, however, the combination of silane or mixture of silanes with a phosphorous precursor may be a more efficient method to increase the corrosion protection and bioactivity of metal coatings.[11] In considering the inorganic components alone, phosphorus may act as a network former in conjunction with silicon to overcome the problem of voids and pores that form during curing of the film as a result of water and ethanol evaporation. The incorporation of phosphorus into bioactive hybrids is an attractive goal in itself with phosphorus playing a relevant role in many biological processes, including osteoblast proliferation.[9] Phosphorous ions could additionally enhance biocompatibility through adsorption of physiological proteins.

This contribution evaluates the bioactivity and corrosion protection properties of novel sol-gel coatings based on the modification of an organic-inorganic (O-I) hybrid (mixture of organofunctional alkoxysilanes γ-methacryloxypropyltrimethoxysilane (MAPTMS) and tetramethylorthosilicate (TMOS)) with a phosphorous precursor (triethylphosphite (TEP)), allowing the introduction of phosphorus at a molecular level into the O-I hybrid network.

Experimental

Preparation of the MAPTMS/TMOS/TEP hybrid sol and deposition on Ti6Al4V alloy

Mixtures of MAPTMS (98%) and TMOS (98%) from Aldrich were used as organopolysiloxane matrix precursors. Anhydrous ethanol (EtOH; absolute grade, Carlo Erba) and deionised water (Elga, Maxima Ultra-Pure Water model, 18.2 MOhm•cm) were used for alkoxysilane hydrolysis at a molar ratio of 1:4 TMOS/MAPTMS. The molar ratio of silane/water/EtOH was 1:3:3. The phosphorous precursor dopant TEP (Fluka, 98%) was added to the prepared MAPTMS/TMOS mixture at a volumetric ratio of 0.3, 0.6 and 0.9 mL TEP per 20 mL MAPTMS/TMOS. The mixture was stirred at 700 rpm for 12 h at RT.

Ti6Al4V disks (2 cm diameter x 0.4 cm thickness and 0.9 cm diameter x 0.4 cm thickness) were ground using grit sand papers starting from 320 to 2000 grit size to achieve a uniform surface. Specimens were rinsed with ddH_2O and ultrasonically cleaned in EtOH for 10 min then dried in air. Hybrid coatings were deposited at ambient temperature by immersion of Ti6Al4V alloys in a freshly prepared sol, holding for 1 min, followed by withdrawal at 9 cm/min using a dip-coater. Coated surfaces were cured for 2 h at of 120°C to remove loosely associated water and avoid decomposition of the organic component in the hybrid.

Characterisation of hybrid organic inorganic MAPTMS/TMOS/TEP films

Sol viscosity was measured at room temperature using a BOHLIN viscometer at a shear rate of 10 s^{-1} at 20°C, with a measuring plate of 40.4 mm and 0.150 mm gap. Wettability was determined by the Sessile drop method, measuring the contact angle of 2 µL of ddH_2O on the surface of the specimen. The optical contact angle measuring instrument OCA-15 Plus controlled by a SCA20 software module from Data Physics and was supplied by Neurtek SA (Spain). Three drops per sample were applied, imaged immediately after positioning and the contact angle calculated by the image analysis system. This was repeated 3 times to allow a mean and standard deviation to be calculated. Coating thickness was measured on half coated samples with a stylus profilometer (Form Talysurf 50 Model, Taylor-Hobson, UK). Linear scans of 1 mm were measured across the step between the uncoated and coated surface. Three different areas of each film were studied and coating thickness expressed as a mean value ± standard deviation.

Thermal characterization was studied by TGA using a SETARAM DTA-TG SETSYS Evolution-1750 system, with α-Al_2O_3 reference. Aliquots of 5 mg of each sample were analysed. The sample and the reference material were heated in air from room temperature to 900°C at a rate of 20°C/min. Structural features of the cured hybrid coatings were characterised by attenuated total reflectance-Fourier transform infrared spectroscopy (ATR-FTIR) using a Nicolet Magna IR 550 infrared spectrophotometer at room temperature. Spectra were recorded between 400 and 4000 cm^{-1} at a resolution of 4 cm^{-1}. For each measurement 8 scans were collected.

^{29}Si MAS NMR spectra of the solid samples were recorded at 79.49 MHz using a Bruker AVANCE-400 spectrometer. The external magnetic field was 9.4 Tesla. All measurements were carried out at 20°C and the samples were spun around the magic angle (54°44' with respect to the magnetic field) at a rate of 10 kHz. The ^{29}Si spectra were obtained with single pulse sequences after excitations with a π/2 pulse lengths of 5 µs, and intervals between successive accumulations (recycle delay) of 10 s. The number of scans was 400; ^{29}Si chemical shift values are given relative to $(CH_3)_4Si$. Deconvolution of the NMR spectra was carried out with the WINFIT program to determine the different components and their contributions.

A JEOL 6500F scanning electron microscope (SEM) with field emission gun was used at an acceleration voltage of 15 kV to examine surface morphology and energy dispersive X-ray analysis (EDXa) was used to determine the chemical composition of the hybrid coatings. Samples for EDXa and SEM were coated with a conductive gold or carbon layer to avoid charging due to the nonconductive nature of the samples.

Protein adsorption, mineralisation and *in vitro* studies of normal human osteoblast culture on MAPTMS/TMOS/TEP hybrid films

Protein adsorption was studied with fibrinogen as the model protein. Samples rinsed with phosphate-buffered saline (PBS, pH 7.4) to rehydrate the surface, were transferred to six well plates (Sarstedt Inc., Germany) before 4 mL of 1 mg/mL fibrinogen solution in PBS was pipetted onto each surface (50 mM Tris/HCl, pH 7.4, 100 mM NaCl, 5 mM $MgCl_2$). Adsorption was allowed to proceed for 1 h at 37°C. Samples were thoroughly rinsed with PBS and ddH_2O 3 times to remove unbound protein and salt residues and then dried at 37°C for 2 h. Adsorbed protein was determined by measuring the protein remaining in solution by the Bradford method, with absorbance measured using a well-plate reader (Tecan, Switzerland) at a wavelength of 595 nm and compared to a standard curve. Three samples of each hybrid powder were studied and results expressed as mean values ± standard deviation.

In vitro bioactivity was assessed for the TEP coatings in simulated body fluid (SBF) solution as described by Kokubo *et al.*[12] The solution was buffered at pH 7.4 using tris(hydroxymethyl) aminomethane/HCl and filtered (0.22 mm Millipore filters) to avoid bacterial contamination. SBF treatment was carried out at 37°C, using a sealed polyethylene container under continuous orbital stirring (600 rpm) in an Ecotron HT incubator. After 15 days immersion specimens were removed from solution, rinsed with ddH_2O and dried at room temperature before analysis by XRD, SEM and EDXa.

In vitro studies were performed on coated and untreated Ti6Al4V substrates using normal human osteoblasts (NHOst cells, Lonza, UK). NHOst cells were cultured at 37°C with 5% CO_2 in osteoblast basal medium (Lonza, UK) supplemented with 10% foetal calf serum, 1% gentamycin sulphate and 1% ascorbic acid. Cultures were initiated and maintained as per the supplier's instructions. Cell viability on the different substrates was assessed using the Neutral-red assay.[13] Coated Ti6Al4V disks (2 cm diameter) were sterilised by exposure to methanol. Discs in six well plates (Sarstedt Inc., UK) were seeded with 2500 cells/cm^2. Discs were incubated under normal conditions with refreshment of the media after 3 days. After 7 days the medium was replaced with RPMI-1640 medium (Lonza, UK) containing 0.01% neutral red dye (Sigma-Aldrich, UK) and the plates incubated for 2 h under normal conditions. Discs were rinsed with PBS and then an equal volume of de-stain solution (1% glacial acetic acid, 50% EtOH) added. Plates were shaken for 20 min and absorbance at 540 nm was read by a micro-plate reader (Tecan, Switzerland). The experiment was repeated 4 times in triplicate and disks without cells were used to correct for dye adsorbed to disks. Cell viability/cytotoxicity data was normalised and assessed using GraphPad Prism v.5, using a one way ANOVA and Tukey's multiple pairwise comparison. A

confidence level of 0.05 was used and the assumption of normality was assessed in each case.

The osteoblast f-actin cytoskeleton and focal adhesion sites were visualised by staining fixed (4% paraformaldehyde) and blocked (10% BSA fraction IV in DPBS with 0.1% TWEEN-20) samples after 7 days of culture under normal conditions on 0.9 mm disks seeded with 2500 cells/cm^2. One unit of Alexa Fluor® 568 phalloidin (Invitrogen, UK) was used to stain f-actin. Monoclonal mouse anti-human vinculin (clone hVIN-1) IgG1 (Sigma-Aldrich, UK) at a concentration of 1:1000 with Alexa Fluor® 488 conjugated goat anti-mouse IgG (Invitrogen, UK) secondary at a concentration of 1:1500 was used to visualize focal adhesion sites. Staining was conducted for 1 h in blocking solution with washing between and after staining with DPBS containing 0.1% TWEEN-20. Vectashield mounting solution (Vector Laboratories, USA) containing 4, 6-diamidino-2-phenylindole was used to stain cell nuclei before imaging with an Olympus DP71 fluorescence microscope.

Corrosion protection behaviour of MAPTMS/TMOS/TEP hybrid films

Corrosion protection behaviour of the O-I hybrid/Ti6Al4V system in an electrochemical cell filled with Kokubo's simulated body fluid (SBF; pH 7.4)[12] was evaluated by applying electrochemical impedance spectroscopy (EIS). For this purpose a potentiostat/galvanostat AutoLab EcoChemie PGSTAT30 (Eco Chemie, Utrecht, the Netherlands) equipped with a FRA2 frequency response analyser module was used. A three electrode setup was applied. The working electrode was the investigated sample with an area of 2.14 cm^2. The reference and the counter-electrodes were a saturated calomel electrode (SCE) and a large size graphite sheet, respectively. Logarithmic frequency scans were carried out by applying sinusoidal wave perturbations of ±10 mV in amplitude, in the range of 10^5-10^{-3} Hz. Five impedance sampling points were registered per frequency decade. The EIS measurements were made at the open circuit potential (OCP) after soaking the O-I hybrid/Ti6Al4V samples in SBF at 37ºC with variable immersion time. The impedance data were analysed using the ZView impedance modelling software version 3.1c (Scribner Associates Inc., NC, USA).[14]

Results and discussion

To understand the influence of TEP incorporation on the properties of the sol and resulting films, rheology was used to measure the viscosity of the sol as this criterion governs some of the properties of the film being deposited. Fig. 1A and Table 1 show the variation of sol viscosity as a function of TEP content.

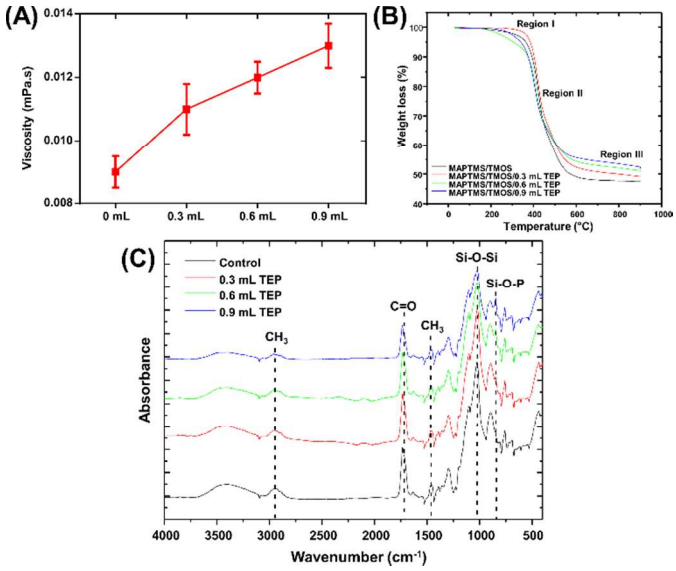

Figure 1. Change in MAPTMS/TMOS sol viscosity as a function of TEP content (A). TGA thermograms of MAPTMS/TMOS hybrids containing different amounts of TEP (B). Representative ATR-FTIR spectra (C) of MAPTMS/TMOS/TEP-Ti6Al4V systems containing: 0, 0.3, 0.6 and 0.9 mL TEP respectively.

Table 1. Sol viscosity, contact angle and thickness of MAPTMS/TMOS coatings on Ti6Al4V substrates as a function of TEP content.

Surface	Contact Angle θ H_2O (°)	Viscosity (mPa.s)	Thickness (μm)
Ti6Al4V	57.4 ± 2.83	-	-
0 mL TEP	67.1 ± 1.17	0.009 ± 0.0005	1.80 ± 0.017
0.3 mL TEP	78.1 ± 0.97	0.011 ± 0.0008	2.14 ± 0.019
0.6 mL TEP	82.1 ± 0.48	0.012 ± 0.0005	2.30 ± 0.052
0.9 mL TEP	85.3 ± 0.41	0.013 ± 0.0007	2.93 ± 0.090

The increase in viscosity with increasing TEP content was attributed to two phenomena: a stronger network due to an increased number of interactions between the phosphorus containing compound and silica in the formed network chains and/or enhancement of the polymerisation of the sol.

Biomaterial wettability is a key factor that affects not only protein adsorption and cell attachment but corrosion in the living body.[15] The water contact angles (θ) determined are shown in Table 1. The decrease in wettability as the concentration of TEP increased could be related to TEP inducing greater cross-linking in the coating; increasing the number of hydrophobic siloxane bonds in the film. An increase in film thickness of the deposited sol-gel with increasing TEP content was also observed (Table 1).

Thermal analysis was used to estimate the stability of the hybrid materials after addition of TEP, Fig. 1B. All the hybrids show an initial weight loss (Region I) attributed to the elimination of the condensation by-products EtOH and water,[16] a second region (Region II) (above 350°C) is attributed to thermal degradation of organic matter and a third region (Region III) (350-900°C) attributed to complete burning of organics and further condensation of silanol groups in the hybrid.[17] Relative thermal stability of the hybrid materials was evaluated from the TGA curves and is reported in Table 2.

Table 2. Thermogravimetric data obtained for MAPTMS-TMOS with TEP.

Sample	Weight loss % at 600°C	Residue % at 900°C
0 mL TEP	50.81	47.51
0.3 mL TEP	47.57	49.21
0.6 mL TEP	46.63	53.18
0.9 mL TEP	44.29	53.63

The trend for thermal stability showed weight loss decreased with increasing TEP addition. This is attributed to phosphorus containing ions acting as a network former resulting in further cross-linking of the inorganic network in the hybrid, the further cross-linking limiting mass loss by silanol condensation at high temperature.

ATR-FTIR spectroscopy was used to study the influence of TEP addition on the structure of the siloxane network. Fig. 1C shows spectra of the prepared films. All spectra show the characteristic Si–O–Si absorption bands of silica at 1013 cm^{-1}, C-H stretching absorptions of the CH_3 residues at 2926 cm^{-1}.[17, 18] The bands at 1454 cm^{-1} correspond to symmetric and asymmetric CH_3 deformation (umbrella) modes.[19, 20] Stretching vibrations of the C=O group at 1738 cm^{-1} arises from the carboxyl of the acrylate group of MAPTMS.[20] The presence of bands corresponding to inorganic silica together with organic groups indicates that after curing of the films at 120°C/2 h both organic and inorganic elements are present in the hybrid coatings. The coating structure was formed by a network of Si–O–Si bonds interrupted by organic groups. In the spectra of MAPTMS/TMOS/TEP coatings, Fig. 1C, the emergence of a new band at 854 cm^{-1} corresponding to Si-O-P bending, which increased in intensity as the amount of TEP in the samples increased was a clear indication of phosphorus incorporation in the silica network.[21] The band observed at 3700–3150 cm^{-1} is characteristic of the stretching vibration of Si–OH.[22] As the amount of TEP in the hybrid increased the Si-OH peak intensity at 3150-3700 cm^{-1} decreased. The consumed -OH may be used in the condensation of TEP hydrolysis products, that results in incorporation of phosphorus containing moieties into the silica network. The spectroscopic findings agreed well with the interpretation of the contact angle measurements, that showed a decrease in wettability as TEP content in the hybrid increased, Table 1.

Solid-state ^{29}Si-NMR measurements were performed to gain further information about the molecular structure of the inorganic network in the prepared O-I hybrids. The ^{29}Si-NMR spectra provide the proportions of T^n (n = 1, 2 or 3) and Q^n (n = 3 or 4) species, where T represents R-Si atoms with n siloxane bonds and Q^3, Q^4 representing the $SiOH(OSi)_3$ and $Si(OSi)_4$ possibilities, allowing quantification of the degree of cross-linking of the siloxane network, Fig. 2.[21]

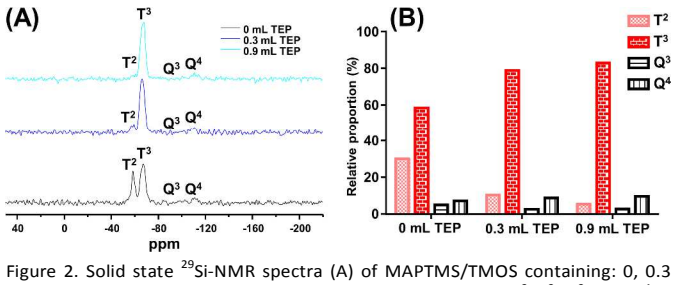

Figure 2. Solid state ^{29}Si-NMR spectra (A) of MAPTMS/TMOS containing: 0, 0.3 and 0.9 mL of TEP. Relationship of the signals (B), for species T^2, T^3, Q^3, and Q^4 in the MAPTMS/TMOS hybrid with varied TEP content.

Both MAPTMS/TMOS and MAPTMS/TMOS/TEP gels (Fig. 2A) exhibited four peaks, with chemical shifts (δ) of −59.6, −67.7, −100.41 and -111.22 ppm, corresponding to T^2, T^3, Q^3 and Q^4 resonances.[21] The proportion of T and Q species in each sol system is given in Fig. 2B. In the MAPTMS/TMOS/TEP gel the T^2 signal decreased in intensity as the content of TEP in the gel increased (Fig. 2A). The presence of TEP in the reaction mixture increased the cross-linking density, increased the amount of fully condensed Si-O-Si structures in the films while decreasing the number of silanol groups. Hybrids with TEP had a larger fraction of T^3 and Q^4 species than the MAPTMS/TMOS sample. The relative intensity (in area) of T^3/T^2 signals is 1.94, 7.66 and 16.15 for xerogels containing 0, 0.3 and 0.9 mL TEP respectively, providing evidence that TEP containing xerogels possess a higher degree of cross-linking. These results correlated with those obtained by ATR-FTIR and contact angle measurements; the presence of phosphorus containing moieties in the hybrid leads to a decrease in silanol groups due to enhanced cross-linking.

Fig. 3A and B shows representative SEM micrographs of the Ti6Al4V alloy and MAPTMS/TMOS film cured at 120°C for 2 h respectively. The formation of smooth, uniform, homogeneous and crack free protective films was observed on the substrates which can be expected to lead to good corrosion resistance for the Ti6Al4V alloys (Fig. 3B). The white points present on the surface may represent condensed silica particles. EDXa showed the presence of carbon, oxygen and silicon together with titanium and aluminium from the substrate. Fig. 3C shows a representative micrograph of the MAPTMS/TMOS/TEP films. EDXa indicated the presence of phosphorus and silicon in the samples. The disappearance of the Ti and Al from the EDXa spectra is attributed to the increased thickness of the coating with TEP addition, Table 1.

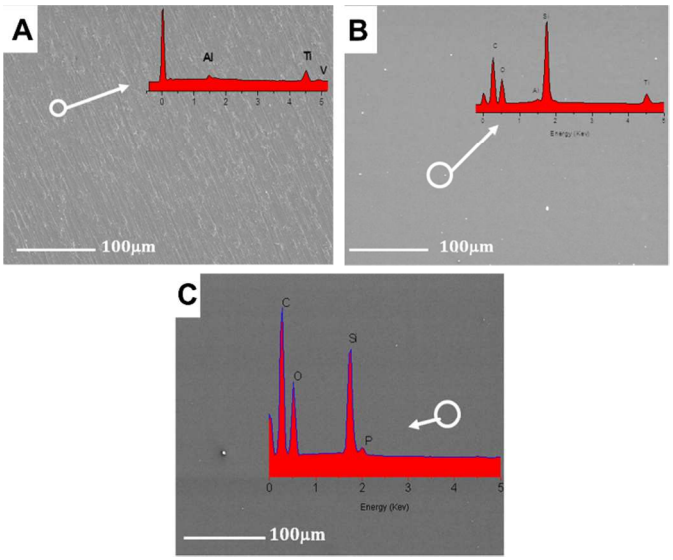

Figure 3. SEM micrographs and EDXa of the prepared hybrid coatings deposited on Ti6Al4V substrates, uncoated (A) and containing 0 (B) and 0.9 mL of TEP (C).

Protein adsorption to MAPTMS/TMOS/TEP hybrid films, mineralisation, osteoblast viability and cytoskeletal studies.

To evaluate the potential use of the prepared coatings for biomedical implants protein adsorption to the surface was

examined, Fig. 4A. Fibrinogen, a serum protein which is of interest in implant integration was selected as the model.[23] Greater amounts of fibrinogen were adsorbed onto MAPTMS/TMOS/TEP-Ti6Al4V systems compared with the MAPTMS/TMOS-Ti6Al4V, and uncoated Ti6Al4V alloy over the same incubation time. Thus, phosphorus incorporation in the films leads to enhancement of protein adsorption. This could be due to the presence of negatively charged phosphorous binding sites for protein adsorption, in this case to the positively charged αC domains of fibrinogen.[24] The ability of the different coatings to induce mineralisation of the surface after exposure to Kobuko's SBF at 37°C for 15 days was checked, which resulted in the formation of a precipitate which could not be conclusively identified as hydroxyapatite (refer to ESI.). Further work would be required to identify the nature of the precipitate, its evolution and its role in tissue integration.

The effects of the coating surface with and without TEP on normal human osteoblasts (NHOst) was qualitatively evaluated *in-vitro* using the neutral red assay. Four different substrates (uncoated Ti6Al4V, MAPTMS/TMOS coated alloy, MAPTMS/TMOS coated alloy with 0.3 and 0.9 mL TEP) were tested after seven days of exposure. Significant differences in the amount of vital dye taken up by the cells between the samples with TEP and those without could be observed, Fig. 4B. NHOst viability was highest on MAPTMS/TMOS/TEP-Ti6Al4V, with increasing cell proliferation correlating with increasing TEP content. Proliferation of NHOst was slowest on the unmodified Ti6Al4V surface with all other substrates showing significantly more growth. The toxicity of the uncoated alloy was higher with respect to the coated surfaces, which may be attributed to the toxicity of vanadium and aluminium released from the alloy which can induce cell toxicity and adverse tissue reactions as reported previously.[25] The decrease of cytotoxicity for the coated surfaces probably arises from the coating which acts as a physical barrier inhibiting ion release to the culture medium. Though previous studies suggested that increasing hydroxyapatite content could improve coating biocompatibility,[11] TEP incorporation yielded a clearer justification for increasing TEP content over using a MAPTMS/TMOS coating alone. For biomaterials, surface composition is known to affect osteoblast adhesion and viability, these results suggest that presence of phosphorus in the coatings promotes osteoblast cell proliferation on the sol-gel coatings and is in agreement with the work of Fike *et al.* who have found that phosphate treatment of osteoblasts increased osteoblast proliferation *in-vitro*.[9]

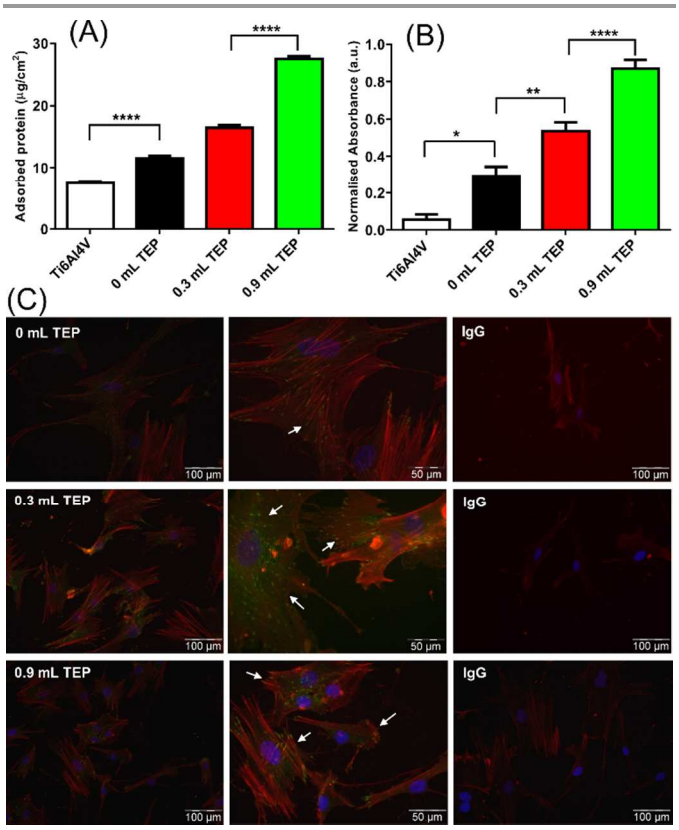

Figure 4. Amount of fibrinogen adsorbed (A) to the uncoated Ti6Al4V, MAPTMS/TMOS-Ti6Al4V and TEP/MAPTMS/TMOS-Ti6Al4V hybrids films containing variable amounts of TEP (0.3-0.9 mL TEP/20 mL of silane mixture). Neutral red proliferation/cytotoxicity assays (B) for NHOst cultured on uncoated Ti6Al4V, MAPTMS/TMOS-Ti6Al4V and TEP/MAPTMS/TMOS-Ti6Al4V hybrids films containing variable amounts of TEP (0.3-0.9 mL TEP/20 mL silane mixture) over a seven day period. Fluorescence micrographs (C) of NHOst on MAPTMS/TMOS-Ti6Al4V and TEP/MAPTMS/TMOS-Ti6Al4V hybrids films containing variable amounts of TEP (0.3-0.9 mL TEP/20 mL silane mixture); vinculin (green), f-actin (red) and nuclei (blue).

Cell morphology was examined by immunofluorescence (IF) microscopy and representative micrographs are shown in Fig. 4C. While osteoblasts were capable of adhesion to all surfaces, fewer cells were observed on the surfaces prepared without TEP. This was most likely to be due to ion dissolution from the alloy which inhibited cell proliferation. The IF imagery was in general agreement with the cell viability assay, Fig. 4B. Phosphorus plays a key role in biochemical pathways in the body, such as energy production, cell division and is known to enhance osteoblast proliferation.[9] In addition it was observed that osteoblasts on all the TEP containing substrates (highlighted points in Fig. 4C) showed a more substantial network of f-actin stress fibres and expression of vinculin than osteoblasts cultured on the bare alloy or MAPTMS/TMOS coated Ti6Al4V alloy. The study of focal adhesion is an indirect measure of cell adhesion, with the number of focal adhesion sites suggesting that cell adhesion on surfaces with higher TEP content appear to be superior to other substrates. Together these findings show that the TEP containing silane films offered the greatest biocompatibility over the seven day period studied. Our results demonstrate that O-I hybrid coatings based on silane and phosphorous precursors can significantly improve the viability of osteoblast cells and reduce the cytotoxicity of the Ti6Al4V surface and would be promising candidates for further biocompatibility studies.

In vitro corrosion protection behaviour

In vitro corrosion and protection studies of the MAPTMS/TMOS/TEP-Ti6Al4V system immersed in Kokubo's simulated body fluid (SBF) were carried out using electrochemical impedance spectroscopy (EIS). Fig. 5 shows impedance spectra of a MAPTMS/TMOS/TEP-Ti6Al4V system with a volumetric ratio of 0.9 mL TEP *vs.* 20 mL of MAPTMS/TMOS sol evaluated after variable immersion times in SBF. Impedance data in the complex plane (i.e. Nyquist plots) (Fig. 5A) and variations of the logarithm of the impedance module and phase angle both against the frequency logarithm (Bode plots, Fig. 5B) are displayed.

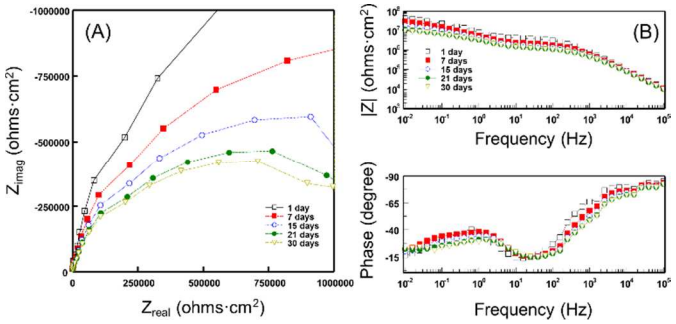

Figure 5. (A) Nyquist and (B) Bode plots of the MAPTMS/TMOS/TEP-Ti6Al4V system (0.9 mL/20 mL of TEP/silane) as a function of immersion time in SBF.

Through qualitative analysis of the impedance plots, valuable information about the intrinsic electrical and protective properties of coatings in aqueous media can be obtained. Thus, from Fig. 5A it can be observed that the diameter of the arc in the high frequency region (HF) of Nyquist plots gradually decreased with immersion time in SBF. The chord located between the two cut-off points of this arc with the real axis of the complex plane coincides with the values of the ionic resistance of the electrolyte inside the pores of the coating, R_{coat}. The decrease of R_{coat} with immersion time indicates that the coating slowly loses its barrier properties.

It is important to note the changes that take place in the corresponding Bode plot, showed a continuous and slow decrease of the impedance modulus especially at low frequencies (Fig. 5B). This behaviour is associated with a slow decrease in the corrosion resistance (R_{corr}) of the metal/coating on the base pores with time during SBF immersion of the MAPTMS/TMOS/TEP-Ti6Al4V system. On the other hand, in Fig. 5C two maxima can be observed in the representation of the phase angle against the frequency logarithm, splitting the Bode plots into two sections; higher frequencies usually containing O-I film information and lower frequencies usually containing information on the metal substrate/O-I film interface.[26]

The EIS results were quantitatively analysed using ZView software.[14] In most cases, the equivalent circuit shown in Fig. 6A displays very good fitting plots for the TEP modified O-I hybrid coating/Ti6Al4V system. Following the notation of the ZView software, the resistor Rs of this equivalent circuit represents the solution resistance of the bulk electrolyte; the capacitor C_{coat} is associated with coating capacitance and R_{coat} is related to the coating pore resistance. R_{corr} and C_{dl} represent the corrosion resistance of the metal substrate and the double layer capacitance at the metal/electrolyte interface respectively, both at the base of pores and damaged areas that develop in the coating during immersion in the corrosive media (SBF).

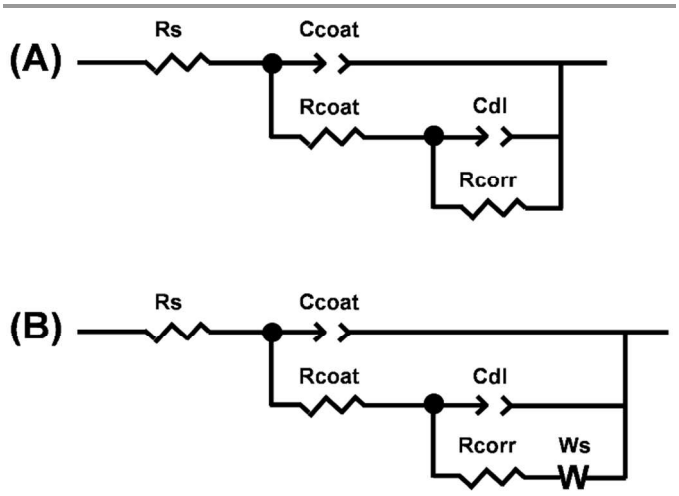

Figure 6. Electrical equivalent circuits proposed for simulating the impedance response of a metal/sol-gel coating system immersed in SBF.

Fig. 7 shows, as an example, the impedance plots obtained experimentally for a MAPTMS/TMOS/TEP-Ti6Al4V sample after 1 h of immersion in SBF. The fitting results generated by applying Zview to the equivalent circuit of Fig. 6A are also plotted. Table 3 shows the fitting values calculated for each of the elements of the equivalent circuit.

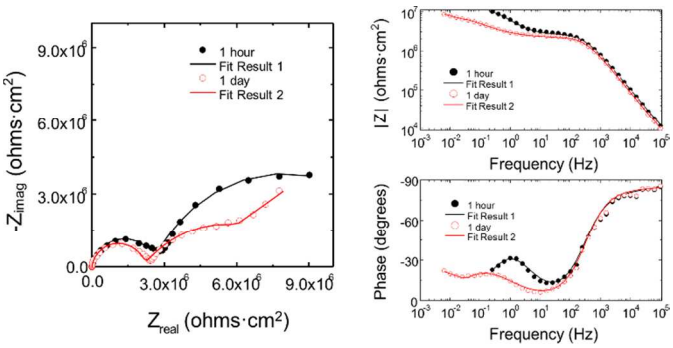

Figure 7. Experimental impedance plots and fit results obtained for a MAPTMS/TMOS/TEP/Ti6Al4V sample by applying equivalent circuit A and B as shown in Fig. 6A and 6B. TEP/silane ratio was 0.9 mL/20 mL and immersion time in SBF was 1 h and 1 day respectively.

Table 3. Values calculated with the Zview software for each element of the equivalent circuit shown in Fig. 7A for the MAPTMS/TMOS/TEP-Ti6Al4V system. TEP/silane ratio 0.9 mL/20 mL. Electrolyte was SBF with an immersion time of 1 h.

Element	Freedom	Value	Error	Error %
Rs	Fixed	30	N/A	N/A
C_{coat}-T	Free(±)	$3.77 \cdot 10^{-10}$	$1.54 \cdot 10^{-11}$	4.08
C_{coat}-P	Free(±)	0.930	$3.79 \cdot 10^{-3}$	0.40
R_{coat}	Free(±)	$3.12 \cdot 10^{6}$	$5.67 \cdot 10^{4}$	1.82
C_{dl}-T	Free(±)	$1.07 \cdot 10^{-7}$	$5.66 \cdot 10^{-9}$	5.26
C_{dl}-P	Free(±)	0.639	$2.80 \cdot 10^{-2}$	4.37
R_{corr}	Free(±)	$8.74 \cdot 10^{6}$	$5.82 \cdot 10^{5}$	6.69
Chi-squared	0.0039			

The criteria used in estimating the quality of the fitting have been evaluated firstly with the lower chi-squared value, and secondly with the lower estimated errors (in per cent) for all components.[27] Good fitting of the values measured over a wide frequency range were obtained for the equivalent circuit.

Nevertheless, sometimes the shape of the low-frequency arcs or tails in the Nyquist diagrams appear to be markedly influenced by diffusion processes.[28] In such cases the equivalent circuit of Fig. 6A is not adequate for modelling and fitting the obtained experimental impedance data. The equivalent circuit shown in Fig. 6B is a modification of the anterior circuit where a new electrical element placed in series with R_{corr}, has been included, the finite-length Warburg impedance, Ws,[29] that takes into account the finite-length diffusion process with transmissive boundary conditions that takes place within pores in the O-I film.[28] Fig. 7 shows an example where it is more appropriate to use the equivalent circuit of Fig. 6B to obtain good fitting results for the low frequency region of the impedance plots. This example corresponds to the impedance plots obtained experimentally for a MAPTMS/TMOS/TEP-Ti6Al4V sample after 1 day of immersion in Kokubo SBF solution.

The evolution of the parameters of the equivalent circuit of Fig. 6B during immersion in Kokubo solution for a MAPTMS/TMOS/TEP-Ti6Al4V system containing 0.9 mL/20 mL TEP/(MAPTMS/TMOS) are shown in Fig. 8 and have been calculated by analysing the impedance plots shown in Fig. 5A-5C. The R_{coat} and R_{corr} values are observed to change mostly within the first 5 days of immersion, and then stay almost constant, within reasonable magnitude margins during the 25 days of immersion in SBF. According to these results, it can be established that these coatings have good protective properties, despite their low thicknesses (< 3 µm). The low values found for the parameter T of the CPE, C_{coat}-T (next to 10^{-10} $ohms^{-1} \bullet s^{-P}$), measured at the beginning of the immersion test in the SBF, indicates that: (i) it is correct to associate the high frequency ark of the Nyquist diagrams to the intrinsic properties of the coating (R_{coat} and C_{coat}); (ii) the equivalent circuit selected (Fig. 6B) to evaluate these results is also correct; (iii) the values found for C_{coat}-T indicate that the coating integrity is suitable and, (iv) this coating presents good dielectric properties acting as an insulating barrier against corrosive media such as SBF. The slow evolution of this parameter with immersion time indicates that water uptake in the coating is low. This behaviour is associated with good barrier properties, good stability and good protective properties of these sol-gel coatings against a corrosive aqueous medium (SBF) and thus against corrosion. The values of the second parameter that defines this CPE, the exponent P (C_{coat}-P), are close to 1 and also decrease slowly with immersion time indicating that the chemical properties of these coatings remain stable during the immersion tests. Concerning the parameter C_{dl}-T, the values obtained are within the range of typical values assigned to the electrochemical double layer on these metallic alloys,[30] which also indicates that the equivalent circuit selected is correct and therefore the middle-frequency arc can be associated with the corrosion processes of the metallic substrate at the base of the coating pores. This process is described by the association in parallel of the R_{corr}/C_{dl} electrical elements in the equivalent circuit. The values of the parameter C_{dl}-P are lower than 1 and quite close to 0.5 (Fig. 8), 1 being the expected value for an ideal capacitor. Due to this fact, these values of C_{dl}-P could be associated with diffusion processes. However, diffusion processes typically take place at very low frequencies, so instead of diffusion processes, it may be more correct to associate the middle-frequency arc of these samples to the electrochemical double layer at the base of the coating pores at the metal/coating interface.

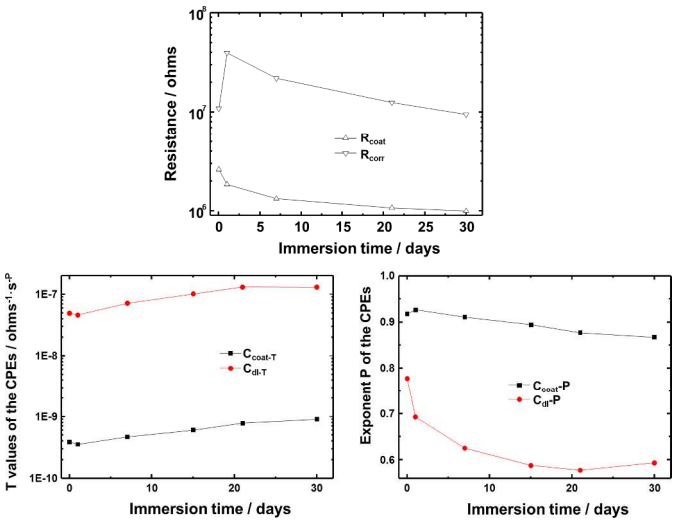

Figure 8. Evolution over 30 days of individual component values of the equivalent circuit shown in Fig. 6B during the immersion tests in Kokubo solution for the MAPTMS/TMOS/TEP-Ti6Al4V system. TEP/silane ratio was 0.9 mL/20 mL.

It is important to note the strong influence of TEP content on the impedance response of the O-I coating in contact with the aggressive media. Fig. 9A shows detail of the Nyquist diagrams obtained after 24 h of immersion in SBF for a bare Ti6Al4V alloy and Ti6Al4V alloy samples coated with O-I films formulated with different concentrations of TEP: 0 (blank), 0.3, 0.6 and 0.9 mL respectively.

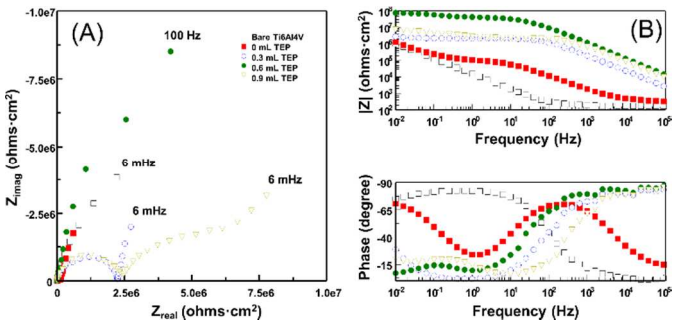

Figure 9. (A) Nyquist and (B) Bode plots of an uncoated Ti6Al4V sample and MAPTMS/TMOS/TEP-Ti6Al4V systems different contents of TEP: 0 mL (blank), 0.3 mL, 0.6 mL and 0.9 mL respectively. The electrolyte was SBF and immersion time 1 day.

Table 4. CPE and resistance values associated with the high frequency arc (HFA) for MAPTMS/TMOS/TEP-Ti6Al4V systems with varying TEP content with SBF electrolyte after one day of immersion.

Sample	$(CPE\text{-}T)_{HFA}$ / $ohms^{-1} \cdot s^{-P}$	$(CPE\text{-}P)_{HFA}$	R_{HFA}/ohms
Uncoated Ti6Al4V	$1.19 \cdot 10^{-5}$	0.91	$1.06 \cdot 10^{7}$
0 mL TEP	$4.31 \cdot 10^{-7}$	0.82	$1.16 \cdot 10^{5}$
0.3 mL TEP	$1.77 \cdot 10^{-9}$	0.91	$2.18 \cdot 10^{6}$
0.6 mL TEP	$2.53 \cdot 10^{-10}$	0.93	$3.89 \cdot 10^{7}$
0.9 mL TEP	$4.03 \cdot 10^{-10}$	0.929	$2.17 \cdot 10^{6}$

The strong dependence of the impedance response versus frequency of these samples makes it difficult to represent the results in the Nyquist format. Fig. 9B shows the same impedance data represented in Bode plot format. It can be clearly observed in Fig. 9A and 9B that the higher impedance values in the entire domain of measured frequencies correspond

to coatings which contain 0.6 and 0.9 mL of TEP. Table 4 shows the values for the different elements of the equivalent circuit. The CPE-T values obtained from the high frequency arc (HFA) of the uncoated Ti6Al4V have the typical order of magnitude of the electrochemical double layer capacitance of a bare metal in contact with an aqueous solution. CPE simulates a non-ideal behaviour of the capacitor due to the passive film formed on the Ti6Al4V surface and R_{HFA} is the R_{corr} resistance associated with it. In contrast with the results obtained for the uncoated Ti6Al4V alloy, the value of the CPE-T from the HFA for the MAPTMS/TMOS-Ti6Al4V system without TEP (blank) is two orders of magnitude lower than the CPEs-T found for the bare metal. This leads us to think that the physical meaning of these CPEs is very different. Effectively, the values of the CPE-T associated with the MAPTMS/TMOS-Ti6Al4V blank sample have the same order of magnitude of those typically expected for the capacitance of porous coatings of low thickness. On the other hand, the values of the capacitance associated to the HFA of the impedance plots obtained for coatings based on sol-gel O-I matrices modified with TEP are two or three magnitude orders less than those associated to the impedance HFA of the 0 mL TEP coating. The order of magnitude of these capacitances are usually associated with dielectric properties of dense thin films with good barrier properties. So it can be established in this case, the resistance R_{HFA} associated in parallel to this CPE_{HFA} corresponds to the resistance of the electrolyte inside the pores of the coating. Consequently, the HFA of the metal/coating systems are associated with two very important intrinsic electrical properties of the coating, C_{coat} and R_{coat}.
In addition, evaluation of these two parameters at different immersion times in the corrosive media provided information on the evolution of the coatings protective properties. Following the criteria above, it can be established that the MAPTMS/TMOS/TEP coatings with lower values of C_{coat}-T and higher values of R_{coat} afford the best protection. Table 4 shows that, for 24 h of immersion in SBF, the coatings containing 0.6 mL of TEP afford the best corrosion protection behaviour. Though the coatings remained adhered to the alloy throughout the biocompatibility and corrosion protection studies, the mechanical adhesion strength of the coatings remains to be directly tested. In comparison to previous work using hydroxyapatite, the performance of the TEP containing coatings was superior by the above criteria.[11] That continued TEP addition did not improve the efficiency of corrosion protection suggests that a point has been reached for this method where further increases in biocompatibility may be detrimental to the other characteristics desirable in the coating. An important consideration for biomaterials design where controls over multiple and potentially conflicting characteristics is required.

Conclusions

Phosphorus (through TEP) can be successfully applied as a network former with silanols by the formation of Si–O–P bonds. Phosphorus incorporation in the siloxane network increased sol viscosity through enhancement of cross-linking and polymerization, as confirmed by NMR. The combination of silane and phosphorous precursor efficiently increases the barrier properties and bioactivity of the films, resulting in an enhancement of protein adsorption and osteoblast viability reflecting the importance of phosphorus for cells. Corrosion protection against aggressive physiological fluids through incorporation of phosphorus also resulted in films with improved protective properties, despite their low thicknesses (< 3 μm). Although higher concentrations of phosphorus supported the greatest biocompatibility, a compromise in the phosphorus concentration used would be required if corrosion resistance was most desirable, though this would still provide a significant enhancement in biocompatibility in comparison to coatings without TEP or the bare alloy alone.

Acknowledgements

This work was supported by the Ministerio de Economía y Competitividad (Project MAT2012-30854). Amir A. El hadad acknowledges a pre-doctoral contract JAE financed by CSIC and Violetta Barranco acknowledges a Ramon y Cajal researcher contract financed by CSIC and MINECO. Part of the studied was financed by the Biomolecular and Materials Interface research Group and the John van Geest Cancer Research Centre at Nottingham Trent University.

Notes and References

[a] Centro Nacional de Investigaciones Metalúrgicas (CSIC), Madrid, Spain.
[b] Instituto de Ciencia de Materiales de Madrid (CSIC), Madrid, Spain.
[c] Universidad Carlos III de Madrid, Departamento de Ciencia e Ingeniería de Materiales e Ingeniería Química, Leganés, Spain.
[d] Interdisciplinary Biomedical Research Centre, School of Science and Technology, Nottingham Trent University, Nottingham, UK, NG11 8NS.
† The authors declare no competing financial interests.
Electronic Supplementary Information (ESI) available: [details of any supplementary information available should be included here]. See DOI: 10.1039/b000000x/

1 M. Ogiso, Y. Yamashita and T. Matsumoto, *J. Dent. Res.,* 1998, **77**, 1426; A. Porter, L. Hobbs, V. Rosen and M. Spector, *Biomaterials*, 2002, **23**, 725; J. Wolke, K. de Groot and J. Jansen, *J. Biomed. Mater. Res.*, 1998, **39**, 524.
2 C. C. Gomes, L. M. Moreira, V. J. S. V. Santos, A. S. Ramos, J. P. Lyon, C. P. Soares and F. V. Santos, *Genet. Mol. Biol.*, 2011, **34**, 116.
3 D. H. Kohn, *Curr. Opin. Solid St. Mater. Sci.*, 1998, **3**, 309; G. J. Thompson and D. A. Puleo, *Biomaterials*, 1996, **17**, 1949.
4 J. M. Gomez-Vega, E. Saiz and A. P. J. Tomsia, *Biomed. Mater. Res.*, 1999, **46**, 549.
5 L. Luo and N. Cui, *J. Alloy Compd.*, 1998, **264**, 299.
6 J. E. Gray and B. Luan, *J. Alloy Compd.*, 2002, **336**, 88
7 R. Supplit, T. Koch and U. Schubert, *Corros. Sci.*, 2007, **49**, 3015; A. L. K. Tan, A. M. Soutar, I. F. Annergren and Y. N. Liu, *Surf. Coat. Technol.*, 2005, **198**, 478; X. Zhong, Q. Li, J. Hu and Y. Lu, *Corros. Sci.*, 2008, **50**, 2304
8 A. A. El hadad, V. Barranco, A. Jiménez-Morales, E. Peon and J. C. Galván, *J. Phys. Conf. Ser.*, 2010, **252**, 012007; J. Gallardo, A. Duran, I. Garcia, J. P. Celis, M. A. Arenas and A. Conde, *J. Sol-Gel Sci. Technol.*, 2003, **27**, 175.

9 J. Fike, B. Cozad, C. R. Fernandez, R. Spears, C. J. Nelson and L. A. Opperman, *IADR/AADR/CADR 87th General Session and Exhibition*., Miami (USA), 2009.
10 M. V. Kahraman, M. Kuğu, Y. Menceloğlu, N. Kayaman-Apohan and A. Güngör, *J. Non-Cryst. Solids*, 2006, **352**, 2143.
11 A. A. El hadad, V. Barranco, A. Jiménez-Morales, E. Peón, G. J. Hickman, C. C. Perry and J. C. Galván, *J. Mater. Chem. B*, 2014, **24**, 3886.
12 T. Kokubo, H. Kushitani, S. Sakka, T. Kitsugi and T. Yamamuro, *J. Biomed. Mater. Res.*, 1990, **24**, 721.
13 G. Repetto, A. del Peso and J. L. Zurita, *Nat. Protoc.*, 2008, **37**, 1125.
14 D. Johnson. Zview for Windows: A software Program for IES Analysis. Version 3.3a. Scribner Associates Inc., NC, USA, Inc., ©1990–2011.
15 N. B. Dahotre, S. R. Paital, A. N. Samant and C. Daniel, *Philos. Trans. R. Soc. A*, 2010, **368**, 1863.
16 S. Yu, T. K. S. Wong, X. Hu and K. Pita, *J. Electrochem. Soc.*, 2003, **150**, F116.
17 C. B. Jing and J. X. Hou, *J. Appl. Polym. Sci.*, 2007, **105**, 697
18 M. Pantoja, B. Díaz-Benito, F. Velasco, J. Abenojar and J. C. del Real, *Appl. Surf. Sci.*, 2009, **255**, 6386; M. A. Rodríguez, M. J. Liso, F. Rubio, J. Rubio and J. L. Oteo, *J. Mater. Sci.*, 1999, **34**, 3867
19 P. Innocenzi and G. Brusatin, *J. Non-Cryst. Solids*, 2004, **333**, 137.
20 A. Franquet, H. Terryn and J. Vereecken, *Appl. Surf. Sci.*, 2003, **211**, 259.
21 H. Niida, M. Takahashi, T. Uchino and T. Yoko, *J. Non-Cryst. Solids*, 2002, **306**, 292.
22 A. A. El hadad, D. Carbonell, V. Barranco, A. Jiménez-Morales, B. Casal and J. C. Galván, *Colloid Polym. Sci.*, 2011, **289**, 1875.
23 S. G. Santos, M. Lamghari, C. R. Almeida, M. I. Oliveira, N. Neves, A. C. Ribeiro, J. N. Barbosa, R. Barros, J. Maciel, M. C. L. Martins, R. M. Goncalves and M. A. Barbosa, *Acta Biomater*., 2013, **9**, 7209.
24 K. E. Healy and P. Ducheyne, *Biomaterials*, 1992, **13**, 553.
25 J. A. Greenwood and J. E. Murphy-Ullrich, *Microsc. Res. Tech.*, 1998, **43**, 420.
26 G. W. Walter, *Corros. Sci.*, 1986, **26**, 681.
27 M. C. Garcia-Alonso, L. Saldana, C. Alonso, V. Barranco, M. A. Munoz-Morris and M. L. Escudero, *Acta Biomater*., 2009, **5**, 1374
28 S. Feliu, J. C. Galván and M. Morcillo, *Progr. Org. Coat.*, 1989, **17**, 143; S. Feliu, J. C. Galván and M. Morcillo, *Corros. Sci.*, 1990, **30**, 989.
29 I. D. Raistrick, D. R. Franceschetti and J. R. Macdonald, in *Impedance Spectroscopy: Theory, Experiment, and Applications*, ed. E. Barsoukov and J. R. Macdonald, John Wiley & Sons, Inc., Hoboken, NJ, USA, 2nd edn., 2005, ch. 2, pp. 27.
30 F. Mansfeld and M. Kendig, in *Organic Coatings: Science & Technology*, ed. G. D. Parfitt and A. V. Patsis, Marcel Dekkar Inc., New York, 1986, ISBN-10: 0824774868

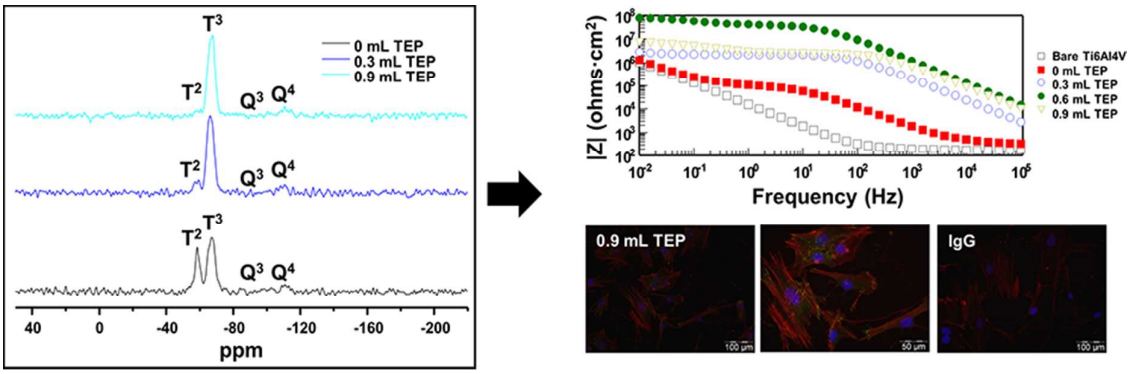

Triethylphosphite was used to introduce phosphorus into organic-inorganic hybrid silica sol-gel coatings prepared using γ-methacryloxypropyltrimethoxysilane and tetramethylorthosilicate. Coatings on Ti6Al4V incorporating triethylphosphite demonstrated greater intermolecular condensation, fibrinogen uptake, *in vitro* biocompatibility and corrosion protection.